Extracting Deciduous Forests Spring Phenology From Sentinel-1 Cross Ratio Index

Huinan Yu, Yajie Yang, Changjing Wang, Rui Chen, Qiaoyun Xie, Guoxiang Liu, and Gaofei Yin, *Senior Member, IEEE*

***Abstract*—Deciduous forests spring phenology plays a major role in balancing the carbon cycle. The cloud cover affects images acquired from optical sensors and reduces their performance in monitoring phenology. Synthetic aperture radar (SAR) can regularly acquire images day and night independent of weather conditions, which offers more frequent observations of vegetation phenology compared to optical sensors. However, it remains unclear how SAR data-derived indices vary across different growth stages of forests. Here, we explored the relationship between the cross ratio (CR) index derived from Sentinel-1 data and the deciduous forest growth process. We proposed a deciduous forests spring phenology extraction method using CR and compared the extracted start of growing season (SOS) with those extracted using normalized difference vegetation index (NDVI) derived from Sentinel-2 optical satellite data and green chromatic coordinate (GCC) derived from ground PhenoCam data. We extracted the SOS of 41 PhenoCam sites over the Continental United States in 2018 using the dynamic threshold method. Our results showed that the variations of CR time series are closely related to the phenological processes of deciduous forests. The SOS extracted using CR data showed high consistency with those extracted using GCC ($R^2 = 0.46$), with slightly lower accuracy compared with NDVI-derived results ($R^2 = 0.62$). Our study illustrates the value and mechanism of deciduous forests spring phenology extraction using SAR data and provides a reference for using SAR data to improve forest phenology extraction in addition to using optical remote sensing data, especially in rainy and cloudy regions.**

***Index Terms*—Cross ratio (CR), deciduous forests, normalized difference vegetation index (NDVI), PhenoCam network, Sentinel-1, spring phenology.**

I. Introduction

SPRING plant phenology is sensitive to climate change and plays a major role in balancing the circulation of carbon, water, and energy between terrestrial ecosystems and the atmosphere [1], [2], [3]. Monitoring spring phenology is an important way to study the effects of global warming on terrestrial ecosystems [1]. Deciduous forests are indispensable for terrestrial carbon storage, and their changes can, in turn, affect climate [4], [5], [6]. Deciduous forests spring phenology, therefore, is a significant indicator of the biological impact of climate change on forests ecosystems [5].

Phenological monitoring can be done at three general scales: in situ, near-surface, and optical-based observations. in situ observations are conducted within small spatial extent, visually assessing phenophases of a limited number of trees and species [7]. The measured phenophases are lack of representativeness, and there are scale differences compared with phenophases obtained by other ways (such as remote sensing). Moreover, the phenological metrics extracted using this method are susceptible to the subjective judgment of observers. in situ observations are difficult to achieve under adverse natural conditions, such as arid desert ecosystems, arctic, and alpine tundra ecosystems [1]. Near-surface sensors mainly collect data depending on conventional or networked red–green–blue (RGB) cameras, which shot repeatedly at high frequency [8]. For instance, "PhenoCams," automated digital time-lapse cameras, can provide a permanent and regular visual record of vegetation conditions [9]. PhenoCam mainly observes terrestrial ecosystems in North America and is one of several networks worldwide that monitor vegetation phenology using near-surface remote sensing [8]. They monitor changes in leaves, canopy, and environmental conditions and quantify phenology by different vegetation indices [10]. Optical-based monitoring is achieved mainly using surface reflectance products that eliminated the effects of the atmosphere on the satellite-measured radiance [11], providing data for extraction of global phenological metrics at a low cost. Compared to traditional course-resolution satellites, e.g., moderate-resolution imaging spectroradiometer (MODIS) and advanced very high resolution radiometer, Sentinel-2 satellite provides decametric resolution data with high revisit frequency, improving our capacity for forest phenology extraction [12], [13].

An accurate detection of the spring plant phenology is key to the global carbon balance [14], plant competition research [15], pest control, and pollen forecasts [16]. Frequent earth observation data are important for accurate estimation of spring phenology. Despite the advantage of providing reflectance spectrum data, the quality of optical satellite data is subject to weather conditions, and cloud contamination makes it difficult to obtain

Manuscript received 24 December 2022; revised 31 January 2023; accepted 14 February 2023. Date of publication 22 February 2023; date of current version 27 March 2023. This work was supported in part by the National Natural Science Foundation of China under Grant 42271323 and Grant 41971282, and in part by the Sichuan Science and Technology Program under Grant 2021JDJQ0007. The work of Q. Xie was supported by the University of Technology Sydney Chancellor's Postdoctoral Research Fellowship. *(Corresponding authors: Qiaoyun Xie; Gaofei Yin.)*

Huinan Yu, Yajie Yang, Changjing Wang, Rui Chen, Guoxiang Liu, and Gaofei Yin are with the Faculty of Geosciences and Environmental Engineering, Southwest Jiaotong University, Chengdu 610031, China (e-mail: hnyu@my.swjtu.edu.cn; yajiey@my.swjtu.edu.cn; wangcj@my.swjtu.edu.cn; chenrui960301@163.com; rsgxliu@swjtu.edu.cn; yingf@swjtu.edu.cn).

Qiaoyun Xie is with the Faculty of Science, University of Technology Sydney, Sydney, NSW 2007, Australia (e-mail: qiaoyun.xie@uts.edu.au).

Digital Object Identifier 10.1109/JSTARS.2023.3247833

high-quality continuous spectral data [17]. For instance, most of phenological changes occur during cloudy periods (spring and autumn) in Mediterranean areas, the capacity of detecting plant growth stage with optical images is significantly limited due to cloud contamination [18]. In addition, the saturation effects of optical satellite data-derived indices cause additional limitation to methods solely based on optical observations [19]. Meanwhile, satellite-based imaging radar offers new opportunity to monitor vegetation phenology, it can regularly acquire images independent of weather conditions due to longer wavelengths than optical remote sensing [18]. Moreover, microwaves have a stronger penetrability and can detect the internal structure of tree canopy, alleviating saturation effects [20].

Synthetic aperture radar (SAR) sensors actively transmit microwaves to earth and then measure the intensity and phase of signal scattered back to the sensor. For example, Sentinel-1 satellites launched by the European Space Agency (ESA) provide frequent observations (six-day temporal resolution) of dual-polarization backscatter data in interferometric wide swath mode (IW) mode. The intensity of microwave signal directly scattered back to the radar antenna is expressed by the backscatter coefficient. Radar backscatter is coaffected by the microwave scattering characteristics of the tree crown and ground surface layer [21]. The SAR backscatter intensity of each part depends on their structure (i.e., the shape, size, and distribution of the scatterers) and dielectric properties [22]. In addition, the microwave's specific properties, such as polarization mode, can also affect backscatter. Many studies on crops [23], [24], [25] and forests [26], [27] have shown that the ratio of C-band cross- and co-polarized backscatter, i.e., cross ratio (CR), is sensitive to vegetation structure and water content. As such, SAR backscatter data could be used to extract phenology because phenology changes (including leaf-out, leaf expansion, and leaf maturation) lead to changes in the structure and dielectric properties of the deciduous forests, resulting in changes in the backscatter properties.

Previous studies on phenology extraction using SAR data mostly focused on croplands [28], [29], [30], [31]. The potential of SAR data for large-scale forest phenology extraction is yet to be investigated [32]. In addition, the physical linkage between the CR dynamics and deciduous forests phenology is unclear [18], [32], [33]. Therefore, it is important to disentangle how CR changes across different growth stages of forest phenology and the drivers of the changes.

In this study, we investigated the potential of SAR data in forest spring phenology extraction in comparison with using traditional optical remote sensing data. The objectives are to: 1) investigate the mechanism of phenology extraction using SAR data; 2) compare phenology extracted through dynamic threshold method using CR derived from SAR data and normalized difference vegetation index (NDVI) derived from optical data at PhenoCam network sites, using phenology extracted from ground-observed green chromatic coordinate (GCC) as a benchmark; and 3) generate spring phenological maps of deciduous forests in the Continental United States and compare phenology observations from Sentinel-1 and Sentinel-2 at continental scale.

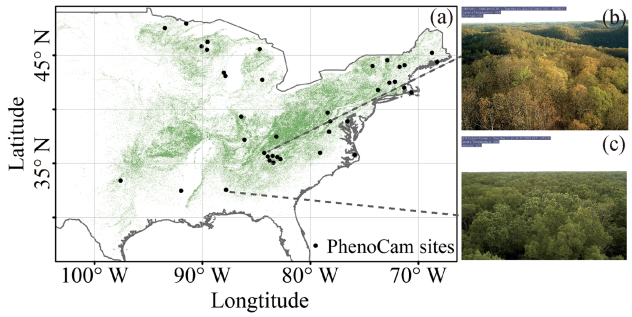

Fig. 1. (a) Spatial distribution of selected PhenoCam deciduous forests sites. Background map illustrates deciduous forests delineated from the United States National Land Cover Database. (b) and (c) Example sites and represent PhenoCam images captured on 01/05/2018 over Robinson (35.96 °N, 84.28 °W) and Russellsage site (32.54 °N, 87.80 °W), respectively.

II. DATA

A. Study Area and PhenoCam Data

This study was conducted at PhenoCam sites located in the United States. The PhenoCam network uses digital camera imagery to monitor ecosystem dynamics over time [34]. Digital cameras in the PhenoCam network provide images in every 30 min, ensuring high-quality data by minimizing data discontinuity under adverse environmental conditions. Image data are three-layer JPEG images with color information stored in red, green, and blue channels. The information about the average intensity of each color channel was extracted based on the user-defined study region to calculate GCC [8]:

$$\mathrm{GCC} = \frac{G_{DN}}{R_{DN} + G_{DN} + B_{DN}} \tag{1}$$

where R_{DN}, G_{DN}, and B_{DN} are the red, green, and blue digital numbers, respectively. GCC describes the proportion of green channel brightness relative to total image brightness, which yield an easily interpreted representation of seasonal changes in canopy status [35].

The heterogeneity of the observed areas affects CR and NDVI. Since the green-up date of deciduous forests in the United States is after March, we excluded sites with a majority of evergreen forests in the observation area based on photos taken by the RGB cameras in February 2018. We selected 41 homogeneous deciduous forests PhenoCam sites (see Fig. 1). See the Appendix for photos of the selected sites. Daily GCC data at these sites in 2018 were used, while Sentinel-1 and -2 data were also available. The robust locally weighted scatterplot smoothing (RLOWESS) [36] and Savitzky–Golay (SG) filtering [37] were successively used to eliminate outliers and reduce noise as they led to the best smooth. The RLOWESS method was performed with a span factor of 15%. A quintic polynomial SG filter with a moving window of nine days was used.

B. SAR Data

In this study, CR calculated using Sentinel-1 SAR data was used to extract spring phenology. As of the time of our study, the Sentinel-1 mission comprises a constellation of two

polar-orbiting satellites (Sentinel-1A and Sentinel-1B), operating day and night performing dual-polarization (VV+VH) C-band SAR imaging. On December 23, 2021, Copernicus Sentinel-1B experienced an anomaly related to the instrument electronics power supply provided by the satellite platform, leaving it unable to deliver radar data. On August 3, 2022, ESA and the European Commission announced that it is the end of the mission for Sentinel-1B. Considering all available orbits (ascending and descending orbits), Sentinel-1 constellation has a high revisit time (2–4 days) due to acquisition overlap [38]. We downloaded all IW mode ground range detected (GRD) high-resolution images (10 m spatial resolution) covering the study areas in 2018 through the Google Earth Engine (GEE) collection "COPERNICUS/S1_GRD" [39]. The Sentinel-1 Toolbox was applied to calibrate and orthocorrect the image to derive backscatter coefficient in decibels (dB). The preprocessing steps implemented by the Sentinel-1 Toolbox are as follows: apply orbit file, GRD border noise removal, thermal noise removal, radiometric calibration, and orthorectification. The details regarding the preprocessings can be found in [38].

C. Optical Satellite Data

Sentinel-2 data were employed for comparison with SAR derived phenology. The Sentinel-2 mission also consists of a constellation of two satellites: Sentinel-2A and Sentinel-2B, which both carry the multispectral instruments. The two satellites allow a repeat cycle of five days and take images in 13 spectral bands at spatial resolutions of 10 m (blue, green, red, near-infrared (NIR) bands), 20 m (three vegetation red edge bands, narrow NIR band, two short-wave infrared (SWIR) bands) and 60 m (coastal aerosol, water vapor, SWIR-Cirrus bands). For Sentinel-2, we used Level-1C imagery, i.e., top of atmosphere (TOA) reflectances from the GEE collection "COPERNICUS/S2." TOA reflectances were used because the top of canopy reflectance products (Level-2A) over America was available only since 2019 at the time of our analysis. All available observations of Sentinel-1 and -2 between January 1, 2018 and December 31, 2018 were downloaded to cover a full phenological cycle.

III. Methods

A. Theoretical Basis

1) C-Band Backscatter Process of Deciduous Forests: For deciduous forests, their structural properties include the size, shape, and orientation distributions of foliage, twigs, branches, and trunks [40]. The dielectric properties of deciduous forests are mainly determined by the water content of trunks, branches, twigs (woody part), and leaves [41]. For the ground surface layer, the backscatter is modulated by its moisture content and material properties (both of which jointly determine dielectric properties) and surface geometry [42].

There are three typical scattering types: surface backscatter from soil and backscatter from branches and trunks, double-bounce backscatter, and volume backscatter from the tree crown [43], [44]. Single polarization is affected by errors associated with the acquisition system (e.g., the radiometric instability) or environmental factors (e.g., variations of soil moisture), which lead to sudden and large fluctuations in backscatter coefficient. CR can reduce these artifacts and is a more robust indicator of forests structure dynamics than σ^0_{VH} or σ^0_{VV} [24], [45]. In addition, other factors leading to sudden and large fluctuation in backscatter coefficient, such as double-bounce effect and different incidence angles, can also be attenuated by CR [24], [33].

2) Spring Resuscitation Process of Deciduous Forests: The growth of deciduous forests is accompanied by changes in its structure and dielectric properties, reflected by changes in CR. Based on other studies on the growth process of deciduous forests, we described the spring resuscitation process of deciduous forests mainly in terms of woody water content and structure change, which can cause changes in scattering characteristics of forests (see Fig. 2). During dormancy, the growth of deciduous forests is inhibited by unfavorable ambient climatic conditions. At this stage, the main scatterers are trunks and branches. Warming during spring prompts a series of biochemical changes in trees to allow for tree resuscitation. Deciduous forests need water to optimally hydrolyze stored macromolecular nutrients and increase enzyme activity [46]. The acropetal transport of water and nutrients begin when buds start developing [47]. Furthermore, the hydrolysis of starch into soluble sugars can modify the osmotic potential and, therefore, intensify the water requirement during bud swelling [48], [49].

3) Hypothesis of Variations in CR During Tree Growth: As such, the water content of branches and trunks, i.e., the woody water content of deciduous forests increases from dormancy to leaf-out [50], [51], results in enhancing backscatter intensity. The main scatterers after leaf-out are the wood and leaves. After leaf-out, the woody water content decreases due to evapotranspiration and reaches its minimum before autumn [50], and results in the decrease of CR. Young leaves continue to grow to a dense mass until the wood is obscured at leaf maturation phase. The leaves have direct and indirect effects on decreasing CR, i.e., leaves directly absorb or forward scatter microwave energy more than backscattering it back, weakening echo energy [52]; the leaves gradually expand until obscure the wood (a strong scatterer), which indirectly causes CR decreasing. At leaf maturation, the woody part is completely obscured by dense leaves and its water content reaches a minimum. At this stage, the main scatterer is the tree crown, volume backscatter is the only backscatter type, and CR reaches the minimum. In autumn, leaves turn yellow and begin to fall, and the woody part gradually revealed. The woody water content gradually increased, but it was not as dramatic as that occurred in spring resuscitation [50], [51]. During leaf senescence, CR gradually increases.

We hypothesize that CR increases before leaf-out and then decreases until leaf maturation, associated with changes in canopy structure and woody water content, and these changes are the theoretical basis for extracting phenological indexes from the CR time series. Based on the above description, the change pattern of CR is shown in Fig. 2.

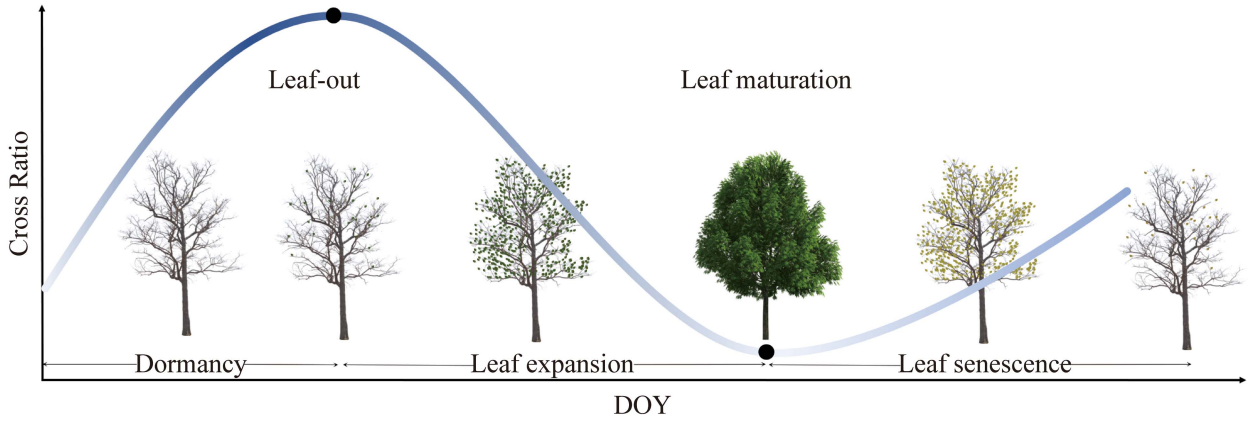

Fig. 2. Variations of phenology phases and woody water content of deciduous forests along with CR values in a year. The curve indicates CR. The change in the color of curve indicates the change in woody water content during the growth of the tree. Dark and light blue indicate high and low woody water content, respectively.

B. Phenology Extraction

For Sentinel-2 data, we excluded cloudy pixels according to the quality control band (QA60 band in "COPERNICUS/S2"), which provides information about clouds and cirrus at the 60 m pixel scale. Then NDVI was calculated using cloud-free data.

The NDVI [53] was calculated as

$$\mathrm{NDVI} = (\mathrm{NIR} - \mathrm{R}) / (\mathrm{NIR} + \mathrm{R}) \tag{2}$$

where R and NIR are reflectance in the red and the NIR bands, respectively.

The Sentinel-1 CR [24] was determined as

$$\mathrm{CR} = \sigma^0_{\mathrm{VH}} - \sigma^0_{\mathrm{VV}} \tag{3}$$

where σ^0_{VH} and σ^0_{VV} are the VH and VV backscatter coefficients, respectively.

For each PhenoCam site, the CR and NDVI were averaged in a 100 m $\times$ 100 m region of interest (ROI) to compare with GCC. The size of the ROI can meet the requirements of observing the scattering characteristics of deciduous forests and also ensure that the observations do not contain scattering from other ground objects. The time series of CR and NDVI at each site were calculated as the mean value of all pixels within the ROI. To eliminate the influence of snowfall, we selected the period of five consecutive days during which the minimum temperature exceeds -5 °C. The temperature data were downloaded from GEE collection "IDAHO_EPSCOR/GRIDMET" [54]. The CR time series without snowfall was then smoothed using RLOWESS and SG methods. The RLOWESS method was performed with a span factor of 30%. A quintic polynomial SG filter with a moving window of nine days was used. The RLOWESS with a span of 2% was applied to smoothen the NDVI time series.

A dynamic threshold method [55] was used to extract the start of season (SOS) from the smoothed GCC, CR, and NDVI time series. SOS extracted from GCC, CR, and NDVI time series were hereafter referred to as "GCC SOS," "CR SOS," and "NDVI SOS," respectively. For GCC and NDVI time series, SOS occurs when the value of the smoothed curve exceeds the minimum plus a given percentage of seasonal amplitude. By contrast, CR decreased gradually after leaf-out until leaf maturation (see Fig. 2). Hence, CR SOS occurs when CR reaches the maximum minus a given percentage of its seasonal amplitude. In order to explore the divergence in phenology extraction among GCC, CR, and NDVI time series, the thresholds spanning from 10% to 50% with a 5% interval are applied over 41 sites. We compared CR SOS and NDVI SOS extracted by different thresholds with GCC SOS as benchmarks. In more detail, we used nine thresholds to extract GCC SOS over 41 sites, and then separately compared the nine sets of GCC SOS with the nine sets of satellite SOS processed by the same extraction procedure. We chose the thresholds of CR SOS and NDVI SOS when they are most consistent with GCC SOS for subsequent applications.

To test the performance of our proposed method for phenological extraction over large geographical range, we generated deciduous forests spring phenological maps of the Continental United States based on CR and NDVI time series using the selected thresholds. The United States National Land Cover Database was applied to delineate deciduous forests areas'. Due to the influence of clouds, a part of pixels in the study area cannot get enough observations in a year. This makes it difficult to generate a phenological map of the Continental United States. To improve the temporal resolution, we downloaded all available satellite data downloaded via GEE for 2018-2021 and then integrated them into an entire seasonal cycle with a six-day resolution.

C. Statistical Analysis

We evaluated the consistency of CR SOS and NDVI SOS with GCC SOS. Three statistical metrics—coefficient of determination [R^2, (4)], the root-mean-square error [RMSE, (5)], and the mean difference of the satellite SOS minus the GCC SOS [BIAS, (6)]—were used to assess the goodness-of-fit, accuracy, and systematic deviation, respectively. These metrics are computed as follows:

$$R^2 = 1 - \frac{\sum_{i=1}^{N} (y_i - y'_i)^2}{\sum_{i=1}^{N} (y_i - \bar{y})^2} \tag{4}$$

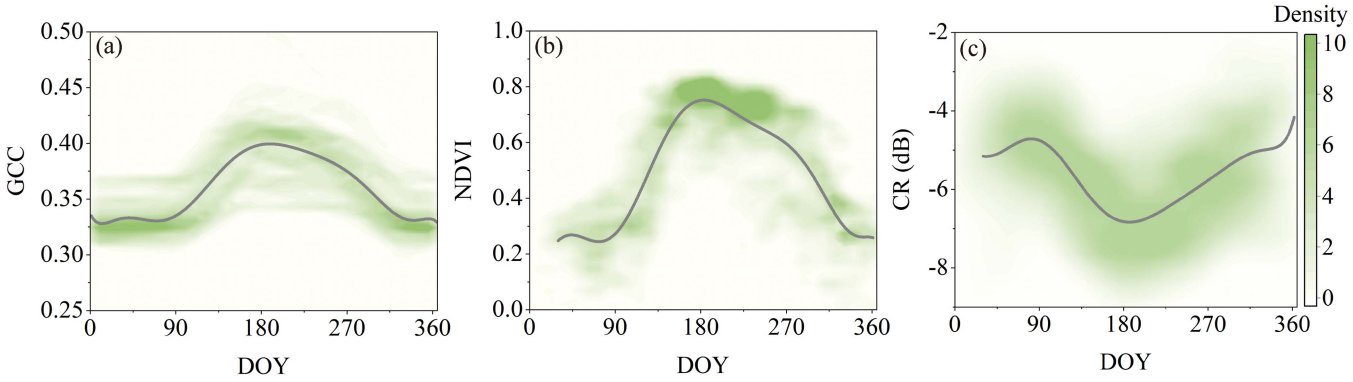

Fig. 3. Time series of (a) GCC, (b) NDVI, and (c) CR for all PhenoCam deciduous forests sites. The gray curves represent the averaged variation of each time series. DOY: Day of year.

$$\mathrm{RMSE} = \sqrt{\frac{\sum_{i=1}^{N} (y_i - y'_i)^2}{N}} \tag{5}$$

$$\mathrm{BIAS} = \frac{1}{N} \sum_{i=1}^{N} (y'_i - y_i) \tag{6}$$

where N is the number of PhenoCam sites, y_i is GCC SOS for the ith site, y_i' is satellite SOS, and $\bar{y}$ is the mean value of GCC SOS for all sites.

IV. Results

A. Time Series of CR

Fig. 3 shows the time series of GCC, NDVI, and CR at 41 deciduous forest sites. The GCC and NDVI time series followed similar seasonal pattern, both began to increase around DOY 90 and reached the peak around DOY 180 [see Fig. 3(a) and (b)]. The actual CR showed an increase until DOY 90 and then decreased and reached its minimum value around DOY 180 [see Fig. 3(c)]. During dormancy, GCC and NDVI remained low, and CR increased and reached its maximum value around DOY 90 as the increase in the woody water content enhanced the woody dielectric properties; during leaf-out to from DOY 90 to 180, GCC and NDVI increased and reached their peak value around DOY 180 caused by increasing leave abundance and greenness, while CR decreased and reached its minimum value around DOY 180 caused by leaf expansion and decreased woody water content; from maturation to the end of season, GCC and NDVI decreased as leaves brown down, while CR increased as woody water content increased. This shows that our assumption for the variation of CR is reasonable (see Fig. 2).

B. Evaluation of SOS Extracted Using Different Data

Fig. 4 shows the correlation statistics between the GCC SOS and satellite SOS under different thresholds over 41 sites. The R^2 between GCC SOS and CR SOS was overall high (averagely 0.44) and independent of the threshold [see Fig. 4(a)], while the R^2 between GCC SOS and NDVI SOS was mostly low (averagely 0.29) except when the threshold used for Sentinel-2 was 50% [see Fig. 4(b)]. The RMSE and BIAS between CR SOS and GCC SOS showed similar patterns across different thresholds compared to the correlations between NDVI SOS and GCC SOS [see Fig. 4(c)–(f)]: the RMSE was lower when both the thresholds used for satellite data and PhenoCam data were higher, while the BIAS was lower when the thresholds used for satellite data and PhenoCam data were closer to each other. The best RMSE and BIAS between GCC SOS and CR SOS were found when the threshold of GCC SOS was about slightly higher than that of CR SOS [see Fig. 4(c) and (e)]. This indicated that the variation of CR time series has a lag compared with the variation of GCC time series after leaf-out. By contrast to the variation patterns of RMSE and BIAS between GCC SOS and CR SOS, GCC SOS lagged behind NDVI SOS in the early growth stage, and the two were gradually consistent after the early growth stage [see Fig. 4(d) and (f)]. This indicated that the change of satellite NDVI time series is faster than that of GCC time series in the early growth stage, and the variation of NDVI and GCC time series is nearly synchronous over time. Fig. 5 shows the variation of CR, GCC, and NDVI at Harvardlph in 2018. The SOS of CR, GCC, and NDVI extracted with thresholds of 10%, 15%, and 30%, respectively, was very close: DOY 109, DOY 111, and DOY 110, respectively. The SOSs of three time series extracted by different thresholds are very close. This further illustrates the aforementioned asynchrony of CR, GCC, as well as NDVI.

C. Comparison of Continental SOS Maps

According to Figs. 4 and 5, the same threshold was not recommended for the consistency of CR SOS and GCC SOS due to the asynchronism between GCC and CR time series. In addition, it is necessary to consider the difference between GCC SOS and NDVI SOS due to the asynchronism between GCC and NDVI time series in the early growth stage. By considering three indicators together, CR SOS30 and NDVI SOS50 were most consistent with GCC SOS50, shown as the red boxes in Fig. 4. The number behind SOS represents the percentage of threshold, e.g., SOS50 represents SOS extracted with a threshold of 50%. Fig. 6 shows the scatterplot for CR SOS30, NDVI SOS50, and GCC SOS50 at 41 PhenoCam sites. The relationship between GCC SOS50 and CR SOS30 showed a moderate consistency and

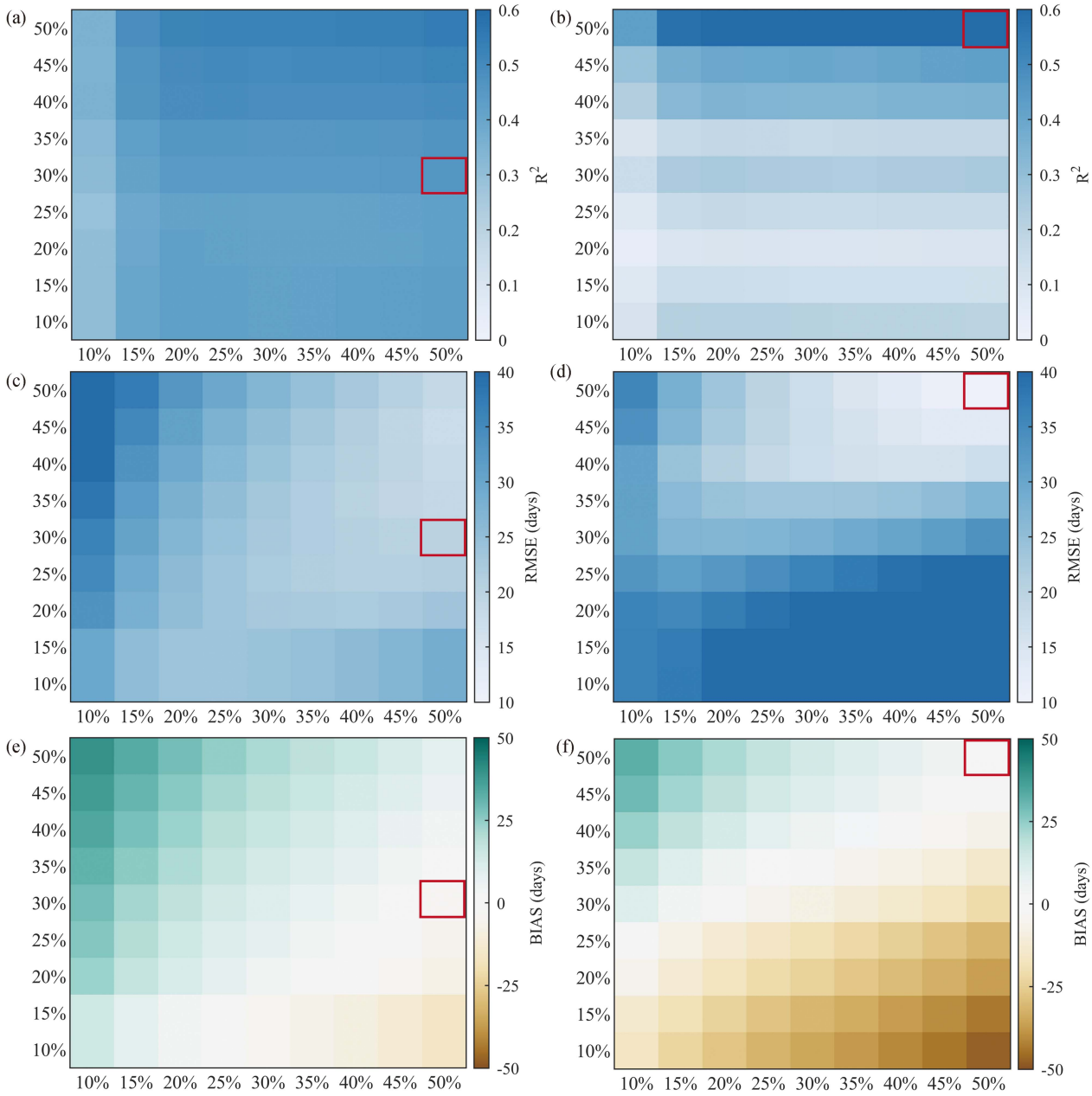

Fig. 4. Comparison of GCC SOS with CR SOS [(a) R^2, (c) RMSE, and (e) BIAS] and NDVI SOS [(b) R^2, (d) RMSE, and (f) BIAS] using different threshold metrics. The red boxes highlight the optimal statistics among GCC SOS50, CR SOS30, and NDVI SOS50.

high uncertainty [$R^2 = 0.46$, RMSE = 20.18 days, and BIAS = -2.15 days, Fig. 6(a)]. GCC SOS50 and NDVI SOS50 showed superior consistency [$R^2 = 0.62$, RMSE = 9.36 days, and BIAS = 1.51 days, Fig. 6(b)]. We generated spring phenological maps for Sentinel-1 and Sentinel-2 based on the above-selected thresholds of 30% and 50%, respectively, as shown in Fig. 7(a) and (b). In general, the CR SOS30 and NDVI SOS50 showed similar spatial patterns at continental scale, and both gradually delayed from low latitude to high latitude. The SOS ranged widely from late March in the south to approximately mid-May in the north. We further counted the satellite SOS by latitude [see Fig. 7(c)]. CR SOS30 and NDVI SOS50 were in good agreement from 32 °N to 47 °N. The standard deviation, within latitude bands, of CR SOS30 was slightly higher than that of NDVI SOS50.

V. Discussion

A. Physiological Drivers of Seasonal Changes in CR in Deciduous Forests

Our study revealed the seasonal change in the CR time series. Previous studies, such as Ling et al. [32], extracted forests phenology based on seasonally changed CR time series. In this study, we related the variation of CR with the variation of structure and water content during the growth of deciduous

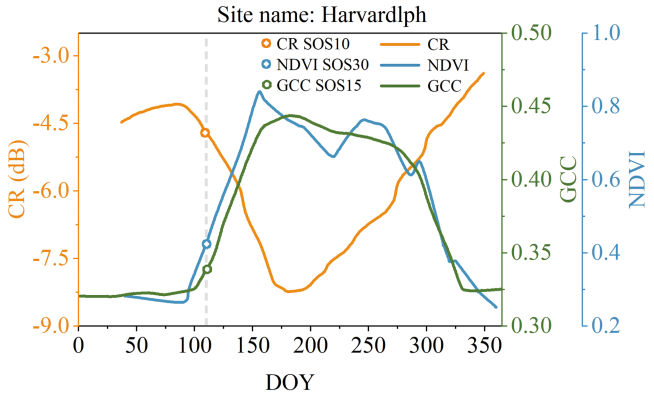

Fig. 5. Variation of CR, GCC, and NDVI at Harvardlph in 2018. The orange, green, and blue circles indicate the SOS of CR, GCC, and NDVI extracted with 10%, 15%, and 30% thresholds, respectively. The gray line indicates DOY 110.

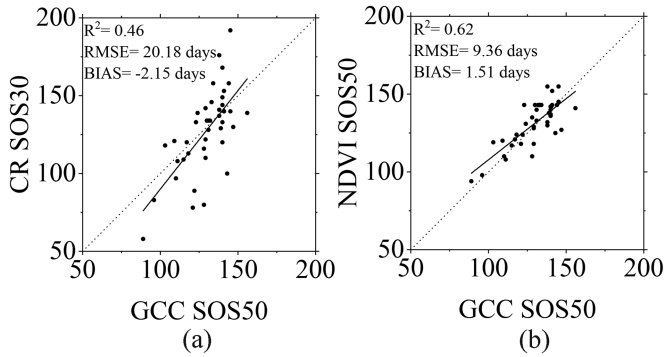

Fig. 6. Comparison of (a) CR SOS extracted with the threshold of 30% (CR SOS30), (b) NDVI SOS extracted with the threshold of 50% (NDVI SOS50) with GCC SOS extracted with the threshold of 50% (GCC SOS50).

forests (see Fig. 2). The results accordingly confirmed our hypothesis in theory (see Fig. 3). This finding helps to further understand the physical significance of CR and further explain the mechanism of extracting phenology based on CR. In the future, the comparison with field measurements of woody water content should be carried out to practically prove the rationality of our hypothesis.

Moreover, we explored the relationship between the timing of CR extremum and specific phenophase. We hypothesized that the CR time series reaches minimum and maximum when leaves mature and leaf-out, respectively (see Fig. 2). Our results showed that the timing when the CR time series reached the minimum is slightly later than the timing when GCC and NDVI reached the maximum (leaf maturation) (see Figs. 3 and 5). This phenomenon may be due to signal saturation, i.e., the sensitivity of optical data to biomass declines earlier than that of SAR data during leaf maturation [24]. The penetrability of microwaves is another reason: C-band microwaves can probe the interior of the tree crown [56], so the sensor can still receive backscatter from a branch within the tree crown after leaf maturation. We suppose that the water content of branches still decreases for a while after leaf maturation due to transpiration until the leaves begin to senesce. At this time, the change of backscatter characteristics of branches can affect CR. The decrease in water content leads to the weakening of dielectric properties and further decrease in CR.

The timing when the CR time series reached the maximum was close to the timing when GCC and NDVI time series began to rise (see Fig. 3). The increase of GCC and NDVI indicated that the emergence of green leaves and greenness began to increase. This confirmed our conjecture and manifested that the timing of the maximum CR time series may be a reliable indicator of spring resuscitation in deciduous forests. Soudani et al. [33] confirmed the high potential offered by Sentinel-1 SAR C-band time series for the detection of forest phenology and their study showed there were obvious extremums in the original time series of polarization combination before smoothing in the early growth stage. Nevertheless, the extremum was neglected and was not further explored.

B. Comparisons Between SOS Derived From GCC, CR, and NDVI

GCC, CR, and NDVI time series all show apparent seasonality (see Fig. 3), although their variations are not completely synchronized, which is partly related to intrinsic differences in the measured signal. The change pattern of statistical indicators between the three extracted SOS (see Fig. 5) was also affected by the measured different signals. We note that the NDVI time series change faster than the GCC time series in the early growth stage. This is because the physical meaning of GCC and NDVI is not exactly the same. GCC is an indicator to characterize vegetation greenness and is mainly sensitive to leaf chlorophyll concentration [10]. NDVI is most strongly influenced by canopy structure rather than by pigments [57]. With the increase of leaf area index associated with the formation of new leaves, NDVI increases more quickly than GCC during the early growth stage, as a result, SOS extracted from GCC time series lags that extracted from NDVI time series.

The change in the CR time series is not synchronous with GCC and NDVI time series, in agreement with Veloso et al. [24]. The timing at which chlorophyll, woody water content, and tree crown structure vary (in response to crop development or weather events) may not perfectly match, causing differences in the synchronicity of GCC, NDVI, and CR time series [31]. Unlike the chlorophyll content that increased rapidly with the growth of young leaves [58], the woody water content decreased slowly after leaf-out [51], thus explaining why CR time series change slower than GCC and NDVI time series. Our study can deepen the understanding of the response of SAR data to deciduous forests growth at the present stage and also provide a new avenue for future research on the phenology based on SAR data.

C. SOS Maps Derived From Satellite Data

We determined the corresponding thresholds of GCC SOS and satellite SOS with optimal consistency according to the statistics (see red boxes in Fig. 5). The process of determining the threshold fully considered the asynchronism between the variation of the woody water content and the variation of leaf greenness of deciduous forests. Previous study on forests phenology used the same threshold to extract phenology from SAR and optical

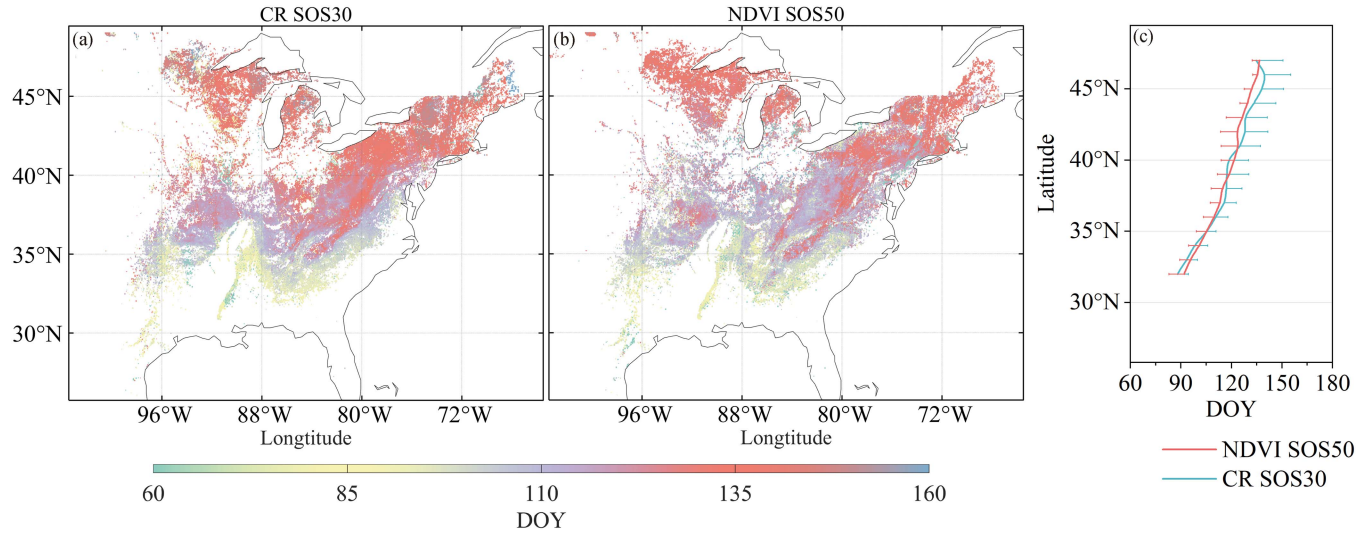

Fig. 7. Continental-scale SOS maps of deciduous forests. (a) CR SOS30 derived from CR. (b) NDVI SOS50 derived from NDVI. (c) Latitudinal gradients of different SOS (32 °N–47 °N). Error bars represent standard deviation. The number behind SOS represents the percentage of threshold. DOY: Day of year.

data [32], without considering the unique characteristics of CR and NDVI. Moreover, our study was carried out based on 41 PhenoCam deciduous forests sites' in the eastern United States, rather than based on few sites [32]. This shows that the method considering different time series characteristics is reliable and stable.

In this study, Sentinel-1 CR time series was used to extract the phenology of deciduous forests based on the continental scale. The CR SOS30 varied with latitude and was in good agreement with NDVI SOS50 as a reference. The spatial patterns of SOS provided by Descals et al. [59] were similar to our results in deciduous forests covering eastern United States. Combined with the advantages of continuous imaging, Sentinel-1 CR time series is expected to extract phenology over a large area suffering from cloudy contamination.

D. Limitations

The uncertainty of CR SOS is high, which may be caused by small fluctuations in the CR time series. Although microwaves are not affected by weather conditions, rain and wind can change the structure and dielectric properties of trees within a short time, which in turn affects the CR time series and could induce noise in the CR data. Wind directly affects the structure, which affects the CR [60]. The effect of rain is that it will add a layer of water to the surface of the observed object, despite that for relatively impermeable objects such as living vegetation, this layer is quite thin. Hobbs et al. [60] showed that the net effect of additional water could in principle reduce the backscatter signal. Therefore, the thin water film may cause increased reflection at the top of the tree crown and reduce multiple backscatters received by the sensor. This phenomenon may also result in uncertainty on phenological phase extraction.

In addition, according to the Appendix, deciduous forests are inevitably mixed with a small amount of evergreen forest at many sites. The scattering characteristics of evergreen forests are different from those of deciduous forests [61], which affects the CR time series and, thus, the phenological extraction results.

Based on other studies on the water content and structure of deciduous forests, this study made assumptions on the changes of CR. Field measurements for structure and woody water content should be carried out in the future to fully verify the hypotheses of this study.

VI. Conclusion

This study investigated the application of SAR satellite data for deciduous forest spring phenology extraction in comparison with optical satellite data, using ground PhenoCam data as a benchmark in the United States. We illustrated that the variation of Sentinel-1 CR time series well tracks the changes in structure and woody water content as deciduous forests grow, providing the rationale for phenology extraction with SAR data. Our results demonstrated the potential of phenology extraction based on the CR index derived from Sentinel-1. The start of the growing season generated using a SAR index CR, derived from Sentinel-1 data, and an optical index NDVI, derived from Sentinel-2 data, showed high accuracy compared with those PhenoCam-derived GCC observations at 41 sites. Furthermore, the United States continental maps of SOS extracted using CR and NDVI time series showed good consistency, indicating large-scale phenology extraction based on SAR data is feasible. Our study provides a reference for improving the capacity for monitoring deciduous forest spring phenology using microwave satellite data, especially in cloudy regions where optical satellite data compromises its observational frequency.

References

[1] A. D. Richardson, T. F. Keenan, M. Migliavacca, Y. Ryu, O. Sonnentag, and M. Toomey, "Climate change, phenology, and phenological control of vegetation feedbacks to the climate system," *Agricultural Forest Meteorol.*, vol. 169, pp. 156–173, 2013.

[2] S. Piao et al., "Plant phenology and global climate change: Current progresses and challenges," *Glob. Change Biol.*, vol. 25, no. 6, pp. 1922–1940, Jun. 2019.

[3] K. Soudani et al., "A survey of proximal methods for monitoring leaf phenology in temperate deciduous forests," *Biogeosciences*, vol. 18, no. 11, pp. 3391–3408, 2021.

[4] J. Penuelas, T. Rutishauser, and I. Filella, "Phenology feedbacks on climate change," *Science*, vol. 324, no. 5929, pp. 887–888, May 2009.

[5] J. M. Hanes, A. D. Richardson, and S. Klosterman, "Mesic temperate deciduous forest phenology," in *Phenology: An Integrative Environmental Science*. New York, NY, USA: Springer, 2013 , pp. 211–224.

[6] N. L. Harris et al., "Global maps of twenty-first century forest carbon fluxes," *Nature Climate Change*, vol. 11, no. 3, pp. 234–240, Mar. 2021.

[7] T. G. Workie and H. J. Debella, "Climate change and its effects on vegetation phenology across ecoregions of Ethiopia," *Glob. Ecol. Conservation*, vol. 13, 2018, Art. no. e00366.

[8] B. Seyednasrollah et al., "Tracking vegetation phenology across diverse biomes using Version 2.0 of the PhenoCam dataset," *Sci. Data*, vol. 6, no. 1, Oct. 2019 , Art. no. 222.

[9] T. B. Brown et al., "Using phenocams to monitor our changing Earth: Toward a global phenocam network," *Front. Ecol. Environ.*, vol. 14, no. 2, pp. 84–93, 2016.

[10] S. Thapa, V. E. G. Millan, and L. Eklundh, "Assessing forest phenology: A multi-scale comparison of near-surface (UAV, spectral reflectance sensor, Phenocam) and satellite (MODIS, Sentinel-2) remote sensing," *Remote Sens.*, vol. 13, no. 8, 2021, Art. no. 1597.

[11] R. E. J. Gray and R. M. Ewers, "Monitoring forest phenology in a changing world," *Forests*, vol. 12, no. 3, 2021 , Art. no. 297.

[12] X. Zhang, J. Wang, G. M. Henebry, and F. Gao, "Development and evaluation of a new algorithm for detecting 30 m land surface phenology from VIIRS and HLS time series," *ISPRS J. Photogramm. Remote Sens.*, vol. 161, pp. 37–51, 2020.

[13] K. Kowalski, C. Senf, P. Hostert, and D. Pflugmacher, "Characterizing spring phenology of temperate broadleaf forests using Landsat and Sentinel-2 time series," *Int. J. Appl. Earth Observ. Geo-Inform.*, vol. 92, 2020, Art. no. 102172.

[14] F.-W. Badeck et al., "Responses of spring phenology to climate change," *New Phytologist*, vol. 162, no. 2, pp. 295–309, May 2004, doi: 10.1111/j.1469-8137.2004.01059.

[15] B. Rathcke and E. P. Lacey, "Phenological patterns of terrestrial plants," *Annu. Rev. Ecol. Syst.*, vol. 16, pp. 179–214, 1985.

[16] C. Traidl-Hoffmann et al., "Impact of pollen on human health: More than allergen carriers?," *Int. Arch. Allergy Immunol.*, vol. 131, no. 1, pp. 1–13, 2003.

[17] J. N. Hird and G. J. McDermid, "Noise reduction of NDVI time series: An empirical comparison of selected techniques," *Remote Sens. Environ.*, vol. 113, no. 1, pp. 248–258, 2009.

[18] R. Proietti et al., "Monitoring spring phenology in Mediterranean beech populations through in situ observation and synthetic aperture radar methods," *Remote Sens. Environ.*, vol. 248, 2020, Art. no. 111978.

[19] T. Manninen, P. Stenberg, M. Rautiainen, P. Voipio, and H. Smolander, "Leaf area index estimation of boreal forest using ENVISAT ASAR," *IEEE Trans. Geosci. Remote Sens.*, vol. 43, no. 11, pp. 2627–2635, Nov. 2005.

[20] M. Hosseini, H. McNairn, A. Merzouki, and A. Pacheco, "Estimation of leaf area index (LAI) in corn and soybeans using multi-polarization C- and L-band radar data," *Remote Sens. Environ.*, vol. 170, pp. 77–89, Dec. 2015.

[21] F. T. Ulaby, K. Sarabandi, K. McDonald, M. Whitt, and M. C. Dobson, "Michigan microwave canopy scattering model," *Int. J. Remote Sens.*, vol. 11, no. 7, pp. 1223–1253, Nov. 1990.

[22] H. Skriver, "Crop classification by multitemporal C- and L-band single- and dual-polarization and fully polarimetric SAR," *IEEE Trans. Geosci. Remote Sens.*, vol. 50, no. 6, pp. 2138–2149, Jun. 2012.

[23] M. Vreugdenhil et al., "Sensitivity of Sentinel-1 backscatter to vegetation dynamics: An Austrian case study," *Remote Sens.*, vol. 10, no. 9, 2018, Art. no. 1396.

[24] A. Veloso et al., "Understanding the temporal behavior of crops using Sentinel-1 and Sentinel-2-like data for agricultural applications," *Remote Sens. Environ.*, vol. 199, pp. 415–426, 2017.

[25] G. Satalino, A. Balenzano, F. Mattia, and M. W. J. Davidson, "C-band SAR data for mapping crops dominated by surface or volume scattering," *IEEE Geosci. Remote Sens. Lett.*, vol. 11, no. 2, pp. 384–388, Feb. 2014.

[26] A. Dostálová, W. Wagner, M. Milenković, and M. Hollaus, "Annual seasonality in Sentinel-1 signal for forest mapping and forest type classification," *Int. J. Remote Sens.*, vol. 39, no. 21, pp. 7738–7760, 2018.

[27] M. Rüetschi, M. Schaepman, and D. Small, "Using multitemporal Sentinel-1 C-band backscatter to monitor phenology and classify deciduous and coniferous forests in Northern Switzerland," *Remote Sens.*, vol. 10, no. 1, 2017 , Art. no. 55.

[28] Y. Song and J. Wang, "Mapping winter wheat planting area and monitoring its phenology using Sentinel-1 backscatter time series," *Remote Sens.*, vol. 11, no. 4, p. 449, 2019.

[29] M. Schlund and S. Erasmi, "Sentinel-1 time series data for monitoring the phenology of winter wheat," *Remote Sens. Environ.*, vol. 246, 2020, Art. no. 111814.

[30] J. Löw, T. Ullmann, and C. Conrad, "The impact of phenological developments on interferometric and polarimetric crop signatures derived from Sentinel-1: Examples from the DEMMIN study site (Germany)," *Remote Sens.*, vol. 13, no. 15, 2021, Art. no. 2951.

[31] M. Meroni et al., "Comparing land surface phenology of major European crops as derived from SAR and multispectral data of Sentinel-1 and -2," *Remote Sens. Environ.*, vol. 253, Feb. 2021, Art. no. 112232.

[32] Y. Ling, S. Teng, C. Liu, J. Dash, H. Morris, and J. Pastor-Guzman, "Assessing the accuracy of forest phenological extraction from Sentinel-1 C-band backscatter measurements in deciduous and coniferous forests," *Remote Sens.*, vol. 14, Jan. 2022 , Art. no. 674.

[33] K. Soudani et al., "Potential of C-band synthetic aperture radar Sentinel-1 time-series for the monitoring of phenological cycles in a deciduous forest," *Int. J. Appl. Earth Observ. Geo-Inform.*, vol. 104, 2021, Art. no. 102505.

[34] A. D. Richardson et al., "Tracking vegetation phenology across diverse North American biomes using PhenoCam imagery," *Sci. Data*, vol. 5, Mar. 2018, Art. no. 180028.

[35] A. D. Richardson, "Tracking seasonal rhythms of plants in diverse ecosystems with digital camera imagery," *New Phytolacca*, vol. 222, no. 4, pp. 1742–1750, Jun. 2019.

[36] W. Cleveland, E. Grosse, and W. M. Shyu, "Local regression models," *Statist. Model.*, pp. 309–376, Jan. 1993.

[37] A. Savitzky and M. J. E. Golay, "Smoothing and differentiation of data by simplified least squares procedures," *Anal. Chem.*, vol. 36, pp. 1627–1639, Jul. 1964.

[38] A. Mullissa et al., "Sentinel-1 SAR backscatter analysis ready data preparation in Google earth engine," *Remote Sens.*, vol. 13, no. 10, 2021, Art. no. 1954.

[39] N. Gorelick, M. Hancher, M. Dixon, S. Ilyushchenko, D. Thau, and R. Moore, "Google earth engine: Planetary-scale geospatial analysis for everyone," *Remote Sens. Environ.*, vol. 202, pp. 18–27, 2017.

[40] M. C. Dobson, F. T. Ulaby, T. LeToan, A. Beaudoin, E. S. Kasischke, and N. Christensen, "Dependence of radar backscatter on coniferous forest biomass," *IEEE Trans. Geosci. Remote Sens.*, vol. 30, no. 2, pp. 412–415, Mar. 1992.

[41] M. A. Karam, A. K. Fung, R. H. Lang, and N. S. Chauhan, "A microwave scattering model for layered vegetation," *IEEE Trans. Geosci. Remote Sens.*, vol. 30, no. 4, pp. 767–784, Jul. 1992.

[42] A. K. Fung and K. S. Chen, "An update on the IEM surface backscattering model," *IEEE Geosci. Remote Sens. Lett.*, vol. 1, no. 2, pp. 75–77, Apr. 2004.

[43] F. Ulaby, R. Moore, and A. Fung, "Microwave remote sensing: Active and passive, Volume III, from theory to applications," pp. 1065–2165, 1986.

[44] E. Attema and F. T. Ulaby, "Vegetation modeled as a water cloud," *Radio Sci.*, vol. 13, no. 2, pp. 357–364, 1978.

[45] S. Khabbazan et al., "Crop monitoring using Sentinel-1 Data: A case study from The Netherlands," *Remote Sens.*, vol. 11, no. 16, 2019, Art. no. 1886.

[46] E. de Faÿ, "Water-related phenomena in winter buds and twigs of picea abies L. (Karst.) until bud-burst: A biological, histological and NMR study," *Ann. Botany*, vol. 86, no. 6, pp. 1097–1107, 2000.

[47] E. Sam and E. Walter, "Water uptake in deciduous trees during winter and the role of conducting tissues in spring reactivation," *IAWA J.*, vol. 7, pp. 31–38, 1986.

[48] A. Cottignies, "The hydrolysis of starch as related to the interruption of dormancy in the ash bud," *J. Plant Physiol.*, vol. 123, no. 4, pp. 381–388, May 1986.

[49] S. Essiamah and W. Eschrich, "Changes of starch content in the storage tissues of deciduous trees during winter and spring," *IAWA J.*, vol. 6, no. 2, pp. 97–106, Jan. 1985 1985.

[50] G. Y. Hao, J. K. Wheeler, N. M. Holbrook, and G. Goldstein, "Investigating xylem embolism formation, refilling and water storage in tree trunks using frequency domain reflectometry," *J. Exp. Botany*, vol. 64, no. 8, pp. 2321–2332, May 2013.

[51] J. M. Young-Robertson, W. R. Bolton, U. S. Bhatt, J. Cristobal, and R. Thoman, "Deciduous trees are a large and overlooked sink for snowmelt water in the boreal forest," *Sci. Rep.*, vol. 6, Jul. 2016, Art. no. 29504.
[52] F. J. Ahern, D. J. Leckie, and J. A. Drieman, "Seasonal-changes in relative c-band backscatter of northern forest cover types," *IEEE Trans. Geosci. Remote Sens.*, vol. 31, no. 3, pp. 668–680, May 1993.
[53] C. J. Tucker, "Red and photographic infrared linear combinations for monitoring vegetation," *Remote Sens. Environ.*, vol. 8, no. 2, pp. 127–150, May 1979.
[54] J. T. Abatzoglou, "Development of gridded surface meteorological data for ecological applications and modelling," *Int. J. Climatol.*, vol. 33, no. 1, pp. 121–131, 2013.
[55] M. A. White, P. E. Thornton, and S. W. Running, "A continental phenology model for monitoring vegetation responses to interannual climatic variability," *Glob. Biogeochem. Cycles*, vol. 11, no. 2, pp. 217–234, Jun. 1997, doi: 10.1029/97GB00330.
[56] H. Omar, M. A. Misman, and A. Kassim, "Synergetic of PALSAR-2 and Sentinel-1A SAR polarimetry for retrieving aboveground biomass in dipterocarp forest of Malaysia," *Appl. Sci.*, vol. 7, pp. 1–20, Jun. 2017.
[57] L. Wingate et al., "Interpreting canopy development and physiology using a European phenology camera network at flux sites," *Biogeosciences*, vol. 12, no. 20, pp. 5995–6015, 2015.
[58] L. Chen et al., "Predicting leaf traits of temperate broadleaf deciduous trees from hyperspectral reflectance: Can a general model be applied across a growing season?," *Remote Sens. Environ.*, vol. 269, 2022, Art. no. 112767.
[59] A. Descals, A. Verger, G. Yin, and J. Penuelas, "A threshold method for robust and fast estimation of land-surface phenology using Google Earth Engine," *IEEE J. Sel. Topics Appl. Earth Observ. Remote Sens.*, vol. 14, pp. 601–606, 2021.
[60] S. E. Hobbs, W. Ang, C. Seynat, and E. S. A. Esa, "Wind and rain effects on SAR backscatter from crops," in *Proc. 2nd Int. Workshop Retrieval Biophys. Geophys. Parameters SAR Data Land Appl.*, 1998, vol. 441, pp. 185–189.
[61] R. Zoughi, J. Bredow, S. Osman, and R. K. Moore, "Fine resolution signatures of coniferous and deciduous trees at C band," *Int. J. Remote Sens.*, vol. 10, no. 1, pp. 147–169, 2007.

Huinan Yu received the M.Eng. degree in surveying and mapping engineering in 2019 from Southwest Jiaotong University, Chengdu, China, where she is currently working toward the Ph.D. degree with the Faculty of Geosciences and Environmental Engineering.

Her research interests include remote sensing of vegetation phenology and vegetation parameter retrieval.

Yajie Yang received the B.S. degree in remote sensing science and technology in 2020 from Southewest Jiaotong University, Chengdu, China, where she is currently working toward the M.S. degree with the Faculty of Geosciences and Environmental Engineering.

Her research interest focusses on remote sensing of vegetation phenology.

Changjing Wang received the M.Eng. degree from Henan Polytechnic University, Jiaozuo, China, in 2020. He is currently working toward the the Ph.D. degree with the Faculty of Geosciences and Environmental Engineering, Southwest Jiaotong University, Chengdu, China.

His research interests include vegetation parameter retrieval and multisource satellite data coordination.

Rui Chen received the B.S. degree in surveying and mapping engineering from the China University of Petroleum (East China), Qingdao, China, in 2019. He is currently working toward the Ph.D. degree with the Faculty of Geosciences and Environmental Engineering, Southwest Jiaotong University, Chengdu, China.

His research interest focusses on topographic correction for optical remote sensing images.

Qiaoyun Xie received the Ph.D. degree in cartography and geographic information system from the Chinese Academy of Sciences and University of Southampton, Beijing and Southampton, China and United Kingdom, in 2017.

She is a Geospatial Scientist, who specializes in vegetation monitoring and their interactions with climate, and currently a Chancellor's Postdoctoral Research Fellow with the School of Life Sciences, Faculty of Science, University of Technology Sydney, Sydney, NSW, Australia. Her main research interest focusses on using satellite data for vegetation monitoring, including vegetation parameter retrieval, vegetation dynamics, vegetation phenology, and their shifting seasonality with climate variability. She also uses airborne remote sensing data and field measurements to observe land surface responses and interactions with climate, land use activities, and major disturbance events.

Guoxiang Liu received the B.E. degree in surveying engineering from the East China Institute of Geology, Jiangxi, China, in 1991, the M.E. degree in geomatics from the Southwest Jiaotong University, Chengdu, China, in 1994, and the Ph.D. degree in remote sensing from The Hong Kong Polytechnic University, Hong Kong, China, in 2003.

He is currently a Professor with the Department of Remote Sensing and Geospatial Information Engineering, Southwest Jiaotong University. From September 2005 to September 2006, he was a Visiting Scholar and conducted research on InSAR with Dr. S. M. Buckley with the Department of Aerospace Engineering and Engineering Mechanics, The University of Texas at Austin, TX, USA. He is the author of 3 books, more than 170 articles, and holds 12 patents. His current research interests include InSAR, PSI, radargrammetry and digital photogrammetry for regional mapping topography, and deformation.

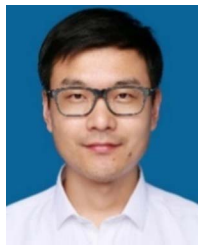

Gaofei Yin (Senior Member, IEEE) received the M.S. degree from Nanjing University, Nanjing, China, in 2011, and the Ph.D. degree from the Institute of Remote Sensing and Digital Earth, Chinese Academy of Sciences (CAS), Beijing, China, in 2015, both in cartography and geographic information system.

From 2015 to 2018, he was a Research Assistant with the Institute of Mountain Hazards and Environment, CAS, Chengdu, China. From 2019 to 2021, he was a Marie Skłodowska-Curie Individual Fellow with Global Ecology Unit, Center for Ecological Research and Forestry Applications, Barcelona, Spain. He is currently a Professor with the Faculty of Geosciences and Environmental Engineering, Southwest Jiaotong University, Chengdu, China. He also serves as an Associated Editor for *IEEE Geoscience and Remote Sensing Letters*. His current research interests include vegetation remote sensing and global change ecology.